# Tell Model Where to Look: Mitigating Hallucinations in MLLMs by Vision-Guided Attention

Jianfei Zhao<sup>1,2</sup>, Feng Zhang<sup>1</sup>, Xin Sun<sup>1</sup>, Chong Feng<sup>1</sup>, Zhixing Tan<sup>3</sup>

<sup>1</sup>Beijing Institute of Technology

<sup>2</sup>Zhongguancun Academy

<sup>3</sup>Tsinghua University

zhqingan@bit.edu.cn

### **Abstract**

Visual attention serves as the primary mechanism through which MLLMs interpret visual information; however, its limited localization capability often leads to hallucinations. We observe that although MLLMs can accurately extract visual semantics from visual tokens, they fail to fully leverage this advantage during subsequent inference. To address this limitation, we propose Vision-Guided Attention (VGA), a training-free method that first constructs precise visual grounding by exploiting the semantic content of visual tokens, and then uses this grounding to guide the model's focus toward relevant visual regions. In image captioning, VGA further refines this guidance dynamically during generation by suppressing regions that have already been described. In VGA, each token undergoes only a single forward pass, introducing a negligible latency overhead of just 4.36%. In addition, VGA is fully compatible with efficient attention implementations such as FlashAttention. Extensive experiments across diverse MLLMs and multiple hallucination benchmarks demonstrate that VGA achieves stateof-the-art dehallucination performance. Further analysis confirms that explicit visual guidance plays a crucial role in enhancing the visual understanding capabilities of MLLMs.

### 1. Introduction

Multimodal Large Language Models (MLLMs) extend the capabilities of large language models (LLMs) into the visual domain, enabling tasks such as visual question answering and image captioning. However, their visual understanding remains limited, as they often exhibit hallucinations—producing outputs that contradict the actual visual content. This hallucination issue significantly affects the

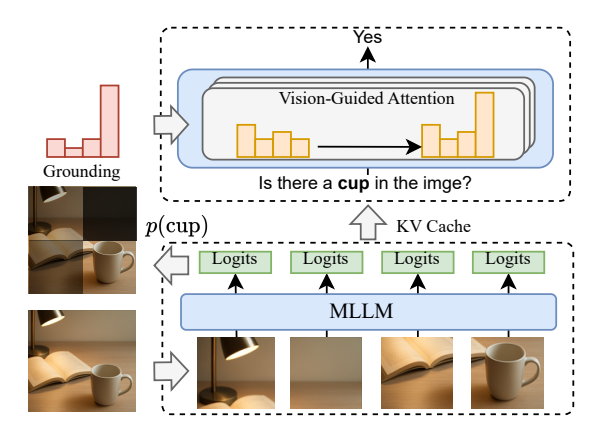


Figure 1. A diagram of vision-guided attention. We first leverage the semantic features embedded in visual tokens to establish visual grounding, and then guide the model's visual attention toward the relevant image regions.

usability and reliability of MLLMs.

Various approaches have been proposed to mitigate hallucinations, such as constructing targeted datasets [21] or designing specialized loss functions [17, 24]. However, the rapid iteration of model architectures has led to diminishing returns for training-based methods. In contrast, training-free hallucination mitigation techniques offer greater practical value due to their plug-and-play nature and strong generalization capability. In particular, a line of research focuses on optimizing visual attention—a mechanism that serves as the primary conduit through which multimodal large language models (MLLMs) interpret visual information [28, 31]—providing one of the most direct pathways to reducing hallucinations.

Previous studies [16, 25, 27, 34] have underscored the essential role of visual attention in MLLMs and shown that strengthening visual attention can substantially mitigate hallucination. However, these approaches depend on the inherent quality of visual attention itself, which is fun-

<sup>&</sup>lt;sup>1</sup>The code is available at: https://github.com/beta-nlp/VGA.

damentally limited in its ability to accurately localize critical visual regions [6, 8], ultimately resulting in suboptimal performance. While employing external tools [35] or performing additional forward passes [3] is feasible, these approaches introduce extra computational overhead and reduce practical usability. Furthermore, because they rely on optimization based on attention distributions, they are incompatible with FlashAttention [4], which does not expose explicit attention weights, thereby restricting their applicability. Consequently, optimizing visual attention remains a significant challenge.

To our surprise, we found that the model can accurately extract semantic features from visual tokens, enabling token-level visual grounding. Based on this observation, we propose Vision-Guided Attention (VGA), a novel strategy for directing visual attention by leveraging the semantic features of visual tokens to identify the most informative ones and allocate greater attention to them. Figure 1 illustrates the overall framework of VGA. More importantly, VGA does not require computing attention weights for individual tokens, making it fully compatible with Flash Attention.

In short, the our main contributions are:

- We introduce Visual Semantic Confidence (VSC), which leverages the semantic features of visual tokens to achieve precise visual grounding.
- We propose Vision-Guided Attention (VGA), which uses the visual grounding produced by VSC to guide visual attention, enabling the MLLM to focus on the most relevant visual tokens.
- VGA is compatible with Flash Attention, and each token requires only a single forward pass, adding just 4.36% inference latency (measured on LLaVA-7B).
- Extensive experiments across diverse benchmarks and multiple MLLMs verify the effectiveness and generalization capability of VGA. Further analysis shows that VSC provides accurate visual grounding; moreover, by leveraging this grounding to guide visual attention, VGA effectively mitigates hallucinations in MLLMs.

## 2. Related Work

Constructing high-quality datasets [2, 21] or designing hallucination-targeted optimization objectives [17, 24] can directly improve model reliability, but the substantial training cost makes these approaches less cost-effective. As a result, training-free dehallucination methods have gained increasing attention. Integrating well-established external tools can effectively enhance the reliability of MLLMs [29, 35], but this also increases the overall system cost. Consequently, optimizing the model's internal representations has become a more appealing alternative. Such methods mitigate hallucinations by adjusting internal components—such as attention weights, logits, or hidden states—to suppress hallucinatory signals. A line of contrastive decoding—based

approaches [9, 12, 30, 32] directly reduces hallucinations in MLLMs by attenuating hallucinatory features in the logits. However, these methods generally require an additional forward pass to activate or expose such features. Other studies [10, 23, 37] edit semantic features in the embedding space to enhance vision-related representations; yet the high dimensionality and complexity of this space make such vector manipulations prone to introducing noise.

Attention mechanisms serve as the primary means by which MLLMs interpret visual features, and the distribution of attention weights offers an intuitive, interpretable reflection of the model's visual behavior. Several studies [16, 36] have directly increased the model's attention to visual content, thereby empirically validating the critical role of visual attention in MLLMs. Other works [5, 26, 33] have investigated functional heterogeneity among attention heads and sought to coordinate their roles accordingly. Additionally, some approaches [8, 27] attribute hallucinations to anomalous attention patterns and propose targeted refinements to address them. While these methods effectively mitigate hallucinations by optimizing visual attention, they largely overlook the inherent variability among visual tokens-specifically, which tokens are most worthy of the model's attention. Some approaches [25, 34] leverage historical attention distributions to assess the importance of visual tokens and use this information to refine the current attention distribution. However, these methods rely entirely on the model's own visual behavior possessing significant limitations. More importantly, optimizing visual attention typically requires access to the full attention distribution in advance, making such approaches incompatible with attention acceleration techniques like Flash Attention [4].

We propose Vision-Guided Attention, which first leverages the semantic features of visual tokens to identify informative tokens and then guide the model's attention to them. Moreover, our method does not rely on attention weights, making it fully compatible with attention acceleration techniques.

### 3. Visual Semantic Confidence

In MLLMs, an input image is first divided into patches, producing visual tokens  $v_1, \cdots, v_m$ . A vision encoder followed by a projector maps each token to a visual embedding  $E_{v_i}$ . These visual embeddings are then concatenated with textual embeddings to form a single sequence, which is fed into the base LLM. The final hidden states are passed through an unembedding matrix to generate logits over the vocabulary. Applying a softmax to the logit at the last position yields the conditional probability for the current generation context, which the model uses to predict the next token:  $p(t_i|t_{< i}) \propto \operatorname{softmax}(\operatorname{logit}_{t-1})$ .

Logits provide a concrete representation of semantic information [7]. The score associated with each token in the

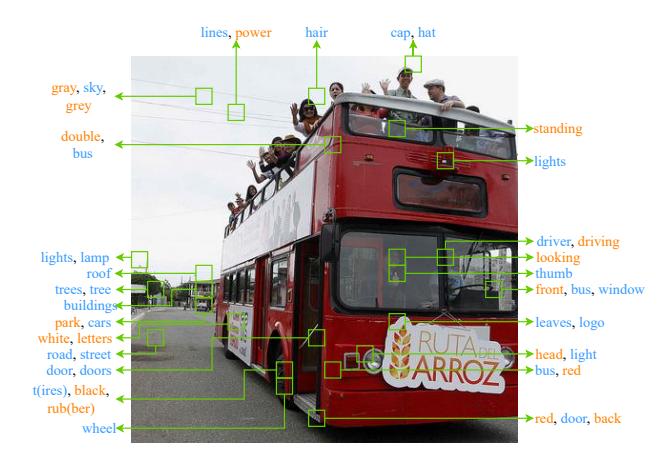


Figure 2. Top-3 tokens in visual logits from LLaVA-7B.

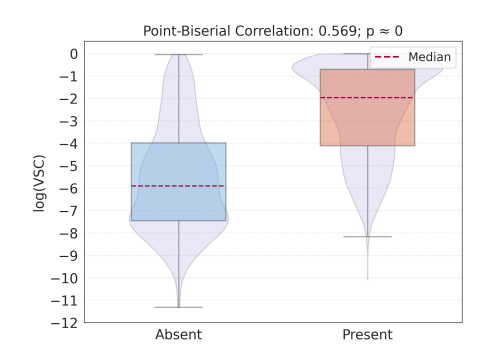


Figure 3. Analysis of visual semantic confidence.

logit vector reflects the model's confidence in selecting that token within the current context. Analogously, visual logits capture the underlying visual semantics of each visual token, as illustrated in Figure 2. We refer to this mechanism in multimodal large language models (MLLMs) as Visual Semantic Confidence (VSC). The score of each word in the visual logits denotes the degree of semantic correlation between that word and the corresponding visual token. Accordingly, aggregating the semantic confidence over all visual tokens for a given word yields that word's overall semantic confidence across the entire image. Consequently, the VSC mechanism enables token-level visual grounding

### 3.1. Object-Directed Grounding

The VSC of a visual token  $v_i$  with respect to an object O is defined as  $c_{v_i}(O) = \operatorname{softmax}[\operatorname{logit}_{v_i}(O)]$ . Given the autoregressive nature of MLLMs, we approximate this confidence using the first token  $o_0$  of the tokenized object O (i.e.,  $c_{v_i}(O) \approx c_{v_i}(o_0)$ ).

We employ an existence-type VQA task to analyze the relationship between the VSC and the object. We represent the semantic confidence of the entire input image with re-

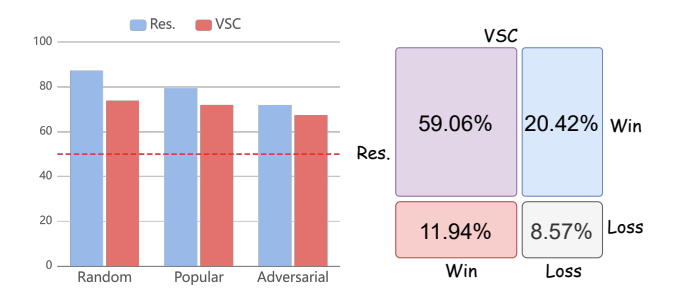


Figure 4. Performance comparison of LLaVA-1.5's response (*Res.*) and its *VSC* on the POPE benchmark.

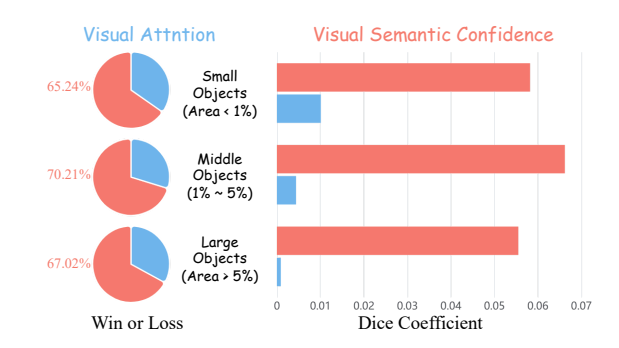


Figure 5. Comparison of visual grounding performance between VSC and the visual attention mechanism of LLaVA-7B. The visual attention maps are extracted from layer 14, following prior work [3].

spect to object O by applying max pooling over all visual tokens:

$$c(O) = \max c_{v_i}(o_0). \tag{1}$$

The threshold of VSC for determining the presence of an object is set to  $\log[c(O)] > -2.5$ . The analysis results are shown in Figure 3. VSC demonstrates a strong correlation with object presence: objects appearing in the image consistently produce higher semantic confidence scores. This finding indicates that VSC effectively captures the visual semantics encoded in the visual tokens.

VSC serves as an intuitive indicator of an MLLM's capacity to interpret visual information. We further examine the consistency between VSC and the model's responses, with results presented in Figure 4. Although object-level judgments derived from VSC are less accurate than the model's own responses, they still demonstrate a correct preference, significantly exceeding 50% accuracy. In addition, we observe that the understanding reflected by VSC does not always fully align with the model's responses, revealing a certain degree of preference discrepancy. These findings suggest that an MLLM's visual understanding is not yet fully exploited, and that the VSC mechanism may be used to enhance the model's visual perception.

Visual tokens associated with an object exhibit higher VSC values with respect to that object. Leveraging this

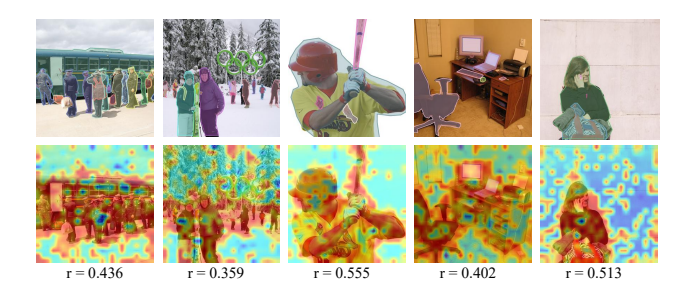


Figure 6. Point-biserial correlation between visual semantic salience and object masks.

property, we obtain the visual grounding of the object as:

$$\mathbf{G}_O = \text{Norm}[\{c_{v_i}(o_0)\}_{i=1}^m] \in \mathbb{R}^m, \tag{2}$$

where m denotes the number of visual tokens, and  $Norm(\cdot)$  represents sum normalization. To quantify the grounding performance of VSC, we employ the Dice Coefficient [18]:

$$D = \frac{2\sum_{i}^{m} c_i g_i}{\sum_{i}^{m} c_i + \sum_{i}^{m} g_i}.$$
 (3)

Here,  $g_i \in [0,1]$  denotes the overlap coefficient between visual token  $v_i$  aand the object's mask annotation. We randomly select 500 images from MSCOCO to evaluate the grounding capability of VSC and compare it with visual attention. The results are shown in Fig. 5. Visual attention suffers from the "sink" phenomenon [8], which limits its grounding ability—particularly for large objects, where it tends to focus only on local regions. In contrast, VSC demonstrates substantially stronger visual grounding performance, exhibiting consistent behavior across objects of different scales. This token-level grounding capability of VSC also provides an indicator of the most informative visual tokens.

# 3.2. Object-Agnostic Grounding

In VQA tasks, a specific object is often explicitly referenced, enabling the use of VSC for precise object grounding. However, this strategy is not applicable to image captioning, which is inherently object-agnostic. Moreover, in image captioning, the model should not concentrate on a single object; instead, it must attend to all visual information in the image—particularly to visual tokens that encode richer visual content.

We assume that visual tokens rich in visual information should exhibit more definite visual semantics. We employ output uncertainty [34, 37] to measure the semantic saliance in visual tokens:

$$c_{v_i} = -\sum_k \log c_{v_i}(w_k) / \log K, \tag{4}$$

where  $\{w_k\}$  are Top-K tokens in  $\operatorname{logit}_{v_i}$ . To distinguish this approach from VSC, we refer to it as Visual Semantic Salience (VSS).

The cases in Figure 6 demonstrate the effectiveness of VSS. We observe that tokens corresponding to distinct objects exhibit higher VSS values, whereas semantically insignificant background regions yield lower VSS. Leveraging this property, we construct visual grounding for all objects present in the image.

### 4. Method

We attribute hallucinations in MLLMs to two primary factors: (1) *Underutilization of extracted visual features*: The model may fail to generate a correct response even when it successfully captures object features with high VSC. (2) *Suboptimal visual attention*: Although visual attention is the main pathway through which the model interprets an input image, it often struggles to accurately focus on the most relevant visual regions. Motivated by these observations, we propose Vision-Guided Attention (VGA), which leverages VSC to establish precise visual grounding and utilizes this grounding to guide the visual attention, thereby directing the model toward the most informative visual tokens.

### 4.1. Vision-Guided Attention

Information interaction among tokens primarily occurs within the self-attention layer:

$$\alpha = \operatorname{softmax}(\frac{\mathbf{Q}\mathbf{K}^T}{\sqrt{d}}) \in \mathbb{R}^{H \times L \times L}.$$
 (5)

Here, K and Q denote the key and query embeddings, H is the number of attention heads and L is the sequence length. The term  $\alpha_{h,i,j}$  represents the attention weight from the i-th token to the j-th token in head h. The model's focus on visual information is reflected in the attention weights assigned to visual tokens by the current generating token, given by  $\alpha_{:-1,s:e}$ . The indices s and e denote the start and end positions of the visual tokens within the sequence, respectively.

Due to the autoregressive nature of MLLMs, we can pre-process the visual tokens to compute the VSC and then leverage the caching mechanism to continue generating the response, ensuring that each token undergoes only a single forward pass. We first use NLP tools to extract the objects mentioned in the question and then construct visual grounding through the VSC. When multiple objects appear in the question, we apply max pooling over the grounding corresponding to all extracted objects:

$$\mathbf{G} = \max_{j} \mathbf{G}_{O_{j}} \in \mathbb{R}^{m}. \tag{6}$$

Here,  $G_{O_j}$  is defined in Eq. (2), and m is the number of visual tokens, satisfying m = e - s. We use G to guide the

model's visual attention:

$$\hat{\boldsymbol{\alpha}}_{h,-1:,s:e} = \boldsymbol{\alpha}_{h,-1:,s:e} + \beta \cdot \mathbf{G},\tag{7}$$

where  $\beta$  is a hyperparameter. The model then applies the guided attention weights to compute self-attention:

$$\hat{\mathbf{z}} = \hat{\boldsymbol{\alpha}} \mathbf{V},\tag{8}$$

where V denotes the value embeddings, and  $\hat{\mathbf{z}}$  represents the self-attention output embeddings.

Attention optimization techniques such as FlashAttention provide high computational efficiency, making them the preferred choice in most MLLM applications. However, these methods do not explicitly output attention weights, which makes a variety of attention-based optimization approaches incompatible with them. Because VGA optimizes attention using visual grounding obtained from VSC, it does not require the computation of attention weights and is therefore fully compatible with FlashAttention.

VGA can be optimized using the associative property of addition:

$$\hat{\mathbf{z}} = (\boldsymbol{\alpha} + \boldsymbol{\beta} \cdot \mathbf{G})V = \mathbf{z} + \boldsymbol{\beta} \cdot \Delta \mathbf{z}, \tag{9}$$

where  $\mathbf{z}$  denotes the output embeddings of vanilla self-attention

### 4.2. Attention Heads Balancing

The multi-head attention mechanism inherently promotes spontaneous specialization among attention heads, resulting in certain heads naturally developing visual functionalities. To prevent disruption to the model's intrinsic visual capabilities, we propose balancing the guidance applied to the attention heads: weaker guidance is applied to the visually specialized heads, while stronger guidance is employed for the non-visual heads. The update for the attention mechanism is formulated as follows:

$$\hat{\mathbf{z}} = \mathbf{z} + \beta \cdot \gamma \cdot \Delta \mathbf{z},\tag{10}$$

where  $\gamma \in \mathbb{R}^H$  represents the balancing coefficients across the attention heads. To approximate the discrepancy in visual functionality across all attention heads, we utilize the similarity between  $\mathbf{z}$  and  $\Delta \mathbf{z}$ :

$$\gamma' = \text{Norm}(\text{sim}(\mathbf{z}, \Delta \mathbf{z})) \in \mathbb{R}^H.$$
 (11)

Here,  $\operatorname{Norm}(\cdot)$  is the sum normalization and  $\operatorname{sim}(\cdot, \cdot) \in [0, 1]$  is the cosine similarity. A higher similarity value for a particular head signifies a more pronounced visual functionality. Finally, we scale this discrepancy to have a mean of 1 and then invert it to obtain the final balancing coefficient

$$\gamma = \text{ReLU}(2 - H \cdot \gamma'), \tag{12}$$

where H is number of attention heads.

### 4.3. Programmed Vision-Guidance

In Visual Question Answering (VQA) tasks, visual demands are typically static and remain unchanged throughout the inference process. In stark contrast, image captioning involves dynamically evolving visual demands as the description is being generated. Consequently, a constant vision grounding mechanism is insufficient to adequately meet the varying visual requirements of image captioning tasks.

To enable visual grounding that dynamically adapts to these changing visual demands during the generation process, we propose the Programmed Visual Grounding (PVG) mechanism. Specifically, during text generation, we dynamically adjust the visual grounding by suppressing regions associated with content that has already been generated.

The adjustment of the visual grounding is performed as follows:

$$\mathbf{G}_{t+1} = (1+\lambda)\mathbf{G}_t - \lambda\mathbf{G}_w,\tag{13}$$

where w is the token generated at the current step and  $\lambda$  is a hyperparameter controlling the adjustment intensity. This adjustment mechanism effectively shifts the vision grounding away from regions associated with already generated content  $\mathbf{G}_w$  and toward regions relevant to the yet-to-begenerated content. Subsequently, the visual grounding is normalized as followed:

$$\mathbf{G}'_{t+1} = \text{Norm}(\text{ReLU}(\mathbf{G}_{t+1})). \tag{14}$$

In image captioning tasks, as more content is generated, the model's dependency on visual information gradually decreases (as observed in [25]). Accordingly, the visual guidance provided to the model is progressively weakened. The attention update mechanism presented in Equation (10) is therefore modified to incorporate this decay:

$$\hat{\mathbf{z}} = \mathbf{z} + ||\mathbf{G}||_0 \cdot \gamma \cdot \beta \cdot \Delta \mathbf{z}. \tag{15}$$

Here,  $||\mathbf{G}||_0$  is the L0 norm of  $\mathbf{G}$ .

# 5. Experiments

### **5.1.** Experimental Setup

**Evaluated MLLMs.** We evaluate the effectiveness of our proposed method, Vision-Guided Attention (VGA), on three representative MLLMs: **LLaVA-1.5** [14], **LLaVA-Next** [15], and **Qwen2.5-VL** [1]. LLaVA-1.5 is available in two sizes: 7B and 13B. Both LLaVA-Next and Qwen2.5-VL are 8B-scale

**Benchmark.** Our method is evaluated on three prominent hallucination benchmarks, covering both Visual Question Answering (VQA) and image captioning tasks: **POPE** [11]:

Table 1. Results on POPE. The results reported as the average performance across the MSCOCO, A-OKVQA, and GQA datasets. **Bolded** values indicates the best results and <u>underlined</u> values indicates the second-best results. *Acc.* stands for Accuracy.

	Method	LLaV	A-7B	LLaVA	A-13B	LLaVA	-Next	Qwen2.5-VL	
		Acc. ↑	F1↑	Acc. ↑	F1 ↑	Acc. ↑	F1↑	Acc. ↑	F1 ↑
	Vanilla	87.12	87.94	84.31	85.96	87.36	85.90	89.88	89.10
	PAI	86.20	87.20	85.36	86.71	87.71	86.34	90.85	90.31
Dandam	$\mathrm{PAI}_{\mathrm{CD}}$	<u>87.27</u>	<u>87.98</u>	86.10	87.24	-	-	-	-
Random	VAF	84.88	86.34	82.42	84.62	89.31	88.45	90.57	89.87
	TARAC	86.99	87.80	87.02	87.80	86.13	84.26	89.79	89.01
	VGA	89.28	89.41	88.58	89.07	89.91	89.21	91.08	90.57
	Vanilla	79.38	82.14	78.64	81.87	85.45	84.14	87.88	87.24
	PAI	78.45	81.56	79.72	82.56	85.95	84.70	87.93	87.65
Domulan	$\mathrm{PAI}_{\mathrm{CD}}$	80.03	82.51	80.86	83.31	-	-	-	-
Popular	VAF	77.13	80.82	77.10	80.91	86.58	85.95	87.90	87.41
	TARAC	79.37	82.10	79.40	82.10	83.94	82.25	87.88	87.22
	VGA	83.51	84.73	84.15	85.50	86.62	86.24	88.06	87.81
	Vanilla	71.85	77.04	71.58	77.23	82.31	81.40	84.82	84.57
Adversarial	PAI	70.83	76.46	72.38	77.64	82.64	81.82	84.60	84.82
	$\mathrm{PAI}_{\mathrm{CD}}$	<u>72.61</u>	<u>77.38</u>	<u>73.44</u>	<u>78.26</u>	-	-	-	-
	VAF	69.59	75.94	70.08	76.41	83.14	83.00	84.80	84.74
	TARAC	71.92	77.03	71.95	77.03	81.04	79.73	84.72	84.47
	VGA	77.02	79.88	77.01	80.28	<u>83.06</u>	83.22	84.86	85.09

Table 2. Results on CHAIR benchmak. Ci and Cs represent the CHAIRi and CHAIRs metric, respectively.

Method	LLaVA-7B			LLaVA-13B			LLaVA-Next			Qwen2.5-VL		
Wiemod	Cs↓	Ci ↓	F1 ↑	Cs ↓	Ci ↓	F1 ↑	Cs ↓	Ci ↓	F1 ↑	Cs↓	Ci ↓	F1 ↑
Vanilla	52.2	13.9	76.1	52.6	14.1	76.4	34.2	9.3	72.2	39.2	9.7	75.0
PAI	33.6	9.0	77.1	40.2	10.8	76.9	34.0	8.9	73.7	36.0	10.3	71.9
$\mathrm{PAI}_{\mathrm{CD}}$	<u>30.8</u>	8.1	<u>76.3</u>	<u>37.0</u>	<u>9.9</u>	77.3	_	-	-	-	-	-
VAF	52.4	14.6	75.3	49.6	13.6	76.5	32.8	<u>8.8</u>	<u>72.6</u>	38.2	9.8	74.8
TARAC	43.0	11.2	75.1	43.0	11.2	75.1	<u>29.8</u>	8.0	71.5	39.8	9.8	74.6
VGA	29.8	<u>8.2</u>	<u>76.3</u>	30.0	8.2	<u>77.1</u>	28.6	8.0	71.6	35.4	9.4	75.1

An object-existence hallucination benchmark designed to assess a model's ability to accurately determine the presence or absence of a specific object in an image. **CHAIR** [20]: Measures object hallucination in image captions by evaluating whether the generated descriptions include objects not present in the input image. **AMBER** [22]: Encompasses three VQA task types targeting existence, attribute, and relational hallucinations. Additionally, AMBER incorporates tests for model-preferable hallucination within the image captioning task.

**Baseline.** We select four existing visual attention-based dehallucination methods for comparative analysis: **PAI** [16]: This method directly amplifies the model's at-

tention weights on visual tokens and further enhances visual features using contrastive decoding. To facilitate a fair comparison of visual attention optimization, we denote the variants with and without contrastive decoding as PAI<sub>CD</sub> and PAI, respectively. **VAF** [27]: Similar to PAI, VAF directly scales up visual attention; however, it also suppresses attention on instruction tokens. **TARAC** [25]: This method quantifies the importance of visual tokens based on attention distributions from previous generation steps and utilizes this information to strengthen the model's focus on relevant visual tokens at the current step.

**Implementation Details.** Following the established practice of PAI, we determine the starting layer for VGA based

on the BOS attention. Specifically, the starting layers are set as follows (with layers numbered from 0): layer 2 for LLaVA-1.5, layer 0 for LLaVA-Next, and layer 4 for Qwen2.5-VL. We terminate VGA application at the middle of the model: at layer 24 for LLaVA-1.5-13B and at layer 16 for all other models. We adopt the default settings of  $\gamma=0.2$  and  $\lambda=0.02$ . For the larger model (LLaVA-1.5-13B) and visually simpler tasks (POPE), we increase  $\gamma$  to 0.25 to apply stronger vision guidance. Stanza [19] is utilized to extract objects mentioned in the question. We employ greedy decoding for next token prediction and set the maximum generation length to 512. All experiments are conducted using a single NVIDIA A800-40G GPU.

### 5.2. Main Results

**POPE.** The experimental results on the POPE benchmark are summarized in Table 1. Our proposed method, VGA, achieves significant improvements in both Accuracy and F1 score, clearly demonstrating its advantage in mitigating existence hallucinations. Moreover, VGA consistently delivers positive gains across all tested MLLMs, highlighting its strong generalizability. While the baselines enhance visual understanding by strengthening the model's attention to visual content, they often lack precise localization of key objects, which leads to suboptimal performance. The superior performance of VGA indicates that providing explicit visual guidance effectively enhances the model's ability to perceive and discriminate objects within the image.

CHAIR. The experimental results on the CHAIR benchmark are presented in Table 2. Our method achieves the overall lowest hallucination rate (i.e., the best Ci and Cs scores) across all evaluated MLLMs, while maintaining no significant drop in F1 score. This result underscores VGA's ability to strike a better balance between generating a richer output and ensuring generation accuracy. Although PAI enhanced by contrastive decoding (PAI<sub>CD</sub>) further refines visual information in the logits and achieves strong performance, contrastive decoding requires two forward passes, which effectively doubles the inference cost. In stark contrast, VGA achieves superior performance with only a single forward pass, demonstrating both higher efficiency and effectiveness.

**AMBER.** AMBER is a comprehensive hallucination benchmark that enables a more thorough evaluation of model hallucinations. The results, shown in Table 3, demonstrate that VGA still achieves significant dehallucination performance, further validating the importance of precise visual guidance. Methods like TARAC and CLVS guide visual attention based on historical attention distributions; however, the localization capability derived solely from visual attention is inherently limited. In contrast, VGA

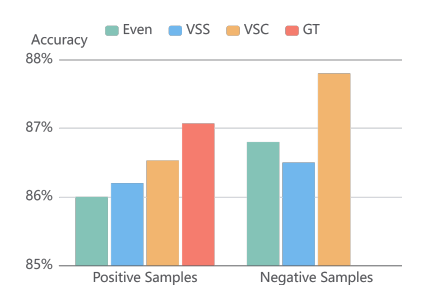


Figure 7. Accuracy on positive and negative samples with different vision-guidance. *Even* denotes uniform attention allocation across all visual tokens, while *GT* refers to the use of ground-truth grounding.

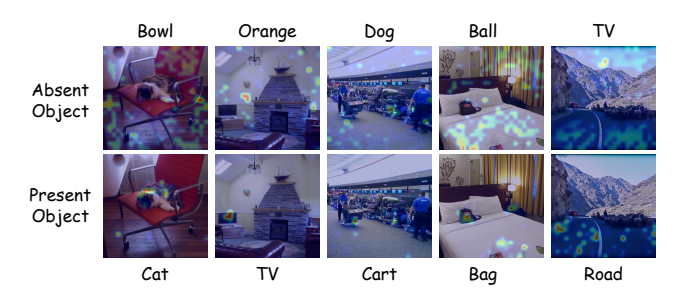


Figure 8. VSC's visual grounding for absent and present objects.

leverages VSC to achieve more accurate visual grounding without relying on external tools, thus enabling a more effective suppression of hallucinations.

# 5.3. Vision-Guidance Enhancing MLLM's Visual Perception

VGA constructs visual grounding using VSC and employs this grounding to guide visual attention, leading to significant performance gains on the POPE benchmark. However, the POPE dataset specifically includes negative samples—that is, instances querying about absent objects. To better understand this behavior and the role of grounding in these challenging cases, we further investigate two critical questions: (1) Why does grounding for absent objects still effectively improve the model's object perception? (2) Can using ground-truth grounding further enhance the model's object perception?

Figure 7illustrates the effects of different visual grounding strategies on both positive and negative samples. First, in positive samples—where the queried object is present—the model's object perception consistently improves as the visual grounding becomes more precise. This demonstrates that, although MLLMs exhibit limited visual localization capability through vanilla attention, providing precise visual grounding effectively enhances their overall visual understanding. Moreover, in negative samples—queries about objects absent from the image—the application of Visual Semantic Confidence still significantly

Table 3. Results on AMBER. The AMBER metric is calculated as (1 - CHAIR + F1)/2.

MLLM	Method	CHAIR↓	Cover ↑	Hal ↓	Cog↓	Acc. ↑	Prec. ↑	Rec. ↑	F1 ↑	AMBER↑
	Vanilla	7.1	50.7	32.5	3.8	72.1	92.2	63.0	74.8	34.35
	PAI	5.8	48.8	27.5	2.5	70.3	94.4	58.8	72.5	33.85
LLaVA-7B	$\mathrm{PAI}_{\mathrm{CD}}$	<u>5.1</u>	48.4	<u>25.7</u>	<u>2.1</u>	<u>73.7</u>	<u>93.1</u>	<u>65.2</u>	<u>76.7</u>	<u>36.30</u>
LLavA-/D	VAF	6.9	50.7	33.0	3.5	68.7	92.6	57.4	70.9	32.50
	TARAC	5.8	<u>49.3</u>	28.5	2.9	72.0	92.8	62.6	74.8	35.00
	VGA	4.5	48.8	21.6	1.9	76.2	<u>93.1</u>	69.3	79.5	38.00
	Vanilla	6.8	51.3	31.1	3.4	71.5	96.0	59.5	73.5	33.85
	PAI	5.4	<u>51.6</u>	<u>27.3</u>	2.1	74.2	<u>95.6</u>	64.0	76.7	36.15
LLaVA-13B	$\mathrm{PAI}_{\mathrm{CD}}$	<u>5.2</u>	52.0	28.3	1.9	<u>75.0</u>	95.3	<u>65.5</u>	<u>77.6</u>	<u>36.70</u>
LLa VA-13D	VAF	6.9	51.2	32.0	3.6	69.5	<u>95.6</u>	56.7	71.2	32.65
	TARAC	5.8	49.3	28.5	2.9	73.0	96.0	61.9	75.3	35.25
	VGA	4.6	49.9	23.6	<u>2.0</u>	78.5	95.0	71.3	81.5	38.95
	Vanilla	7.8	63.1	46.1	3.9	85.9	86.5	93.4	89.8	41.50
	PAI	<u>7.1</u>	64.2	42.2	<u>3.2</u>	<u>86.4</u>	87.4	93.0	<u>90.1</u>	<u>42.00</u>
LLaVA-Next	VAF	7.8	<u>63.2</u>	45.4	3.9	86.0	<u>87.7</u>	91.9	89.7	41.45
	TARAC	6.7	60.3	37.5	3.4	85.8	86.3	93.5	89.8	42.05
	VGA	<u>7.1</u>	62.2	<u>41.4</u>	3.1	86.6	88.4	92.0	90.2	42.05
	Vanilla	<u>4.8</u>	<u>64.8</u>	25.9	1.5	86.5	87.3	93.2	90.1	43.15
	PAI	7.1	60.3	34.7	1.6	86.0	<u>88.1</u>	91.2	89.6	41.75
Qwen2.5-VL	VAF	4.7	64.2	<u>25.1</u>	<u>1.4</u>	85.7	87.1	92.1	89.5	42.90
	TARAC	<u>4.8</u>	65.2	26.5	1.5	<u>86.6</u>	87.8	<u>92.7</u>	<u>90.2</u>	<u>43.20</u>
	VGA	4.7	61.8	24.2	1.3	87.1	88.5	92.5	90.5	43.40

improves the model's ability to correctly reject the presence of such objects. Figure 8 presents the VSC-based grounding maps for both present and absent objects. We find that VSC enhances the model's perception for absent objects by redirecting attention toward low-semantic regions (i.e., background or uninformative areas), allowing the model to correctly infer the object's absence. In contrast, when guided by VSS-based grounding—which directs attention toward visually richer regions—the model is more likely to misinterpret background patterns as spurious evidence of the queried object, thereby leading to hallucinatory responses.

# **5.4. Programmed Vision-Guidance for Image Captioning**

For the image captioning task, we first construct visual grounding based on VSS. Subsequently, we dynamically adjust this guidance during generation by suppressing already-described visual regions—a process we term programmed vision-guidance. As illustrated in Figure 9, the precise grounding capability enabled by Visual Semantic Confidence facilitates the accurate editing of visual guidance. This mechanism effectively steers the model to focus more on previously undescribed regions, promoting comprehensive and non-redundant caption generation.

We conduct an ablation study comparing Programmed

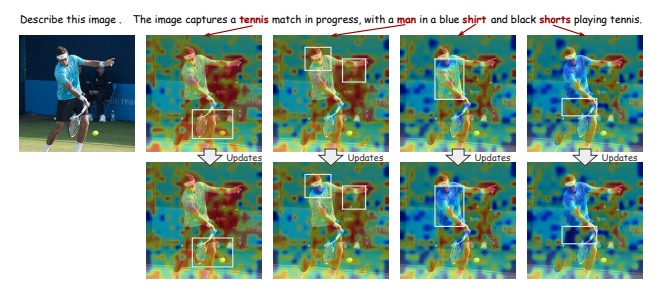


Figure 9. Programmd Vision-Guidance. We set  $\gamma$  to 0.1 in this case to better illustrate the dynamic process.

Vision-Guidance with static VSS-based grounding, with the results presented in Table 4. First, guiding the model to focus on semantically rich regions effectively improves image captioning quality by encouraging the generation of more meaningful and informative content. Conversely, increasing attention to low-semantic regions not only leads to a rise in hallucinations but also results in a decline in recall, as the model generates less relevant or redundant descriptions. Moreover, models operating without dynamic adjustment of visual guidance tend to produce more concise descriptions. While this static approach may reduce hallucination rates, it concurrently leads to the omission of important visual de-

Table 4. PVG represents Programmed Vision-Guidance. Reversed VSS denotes initial vision guidance by  $1 - \mathbf{G}$  in Eq. (2).

Setting	Cs	Ci	R	F1
VGA	29.8	8.2	<b>70.4</b> 69.5 65.0	76.3
Reversed VSS	30.6	8.6	69.5	75.9
w/o PVG	22.2	5.6	65.0	74.5

tails. In summary, Programmed Vision-Guidance significantly enhances MLLM performance in image captioning. It achieves this by balancing detail preservation and hallucination suppression through adaptive visual grounding, thereby mitigating the trade-off inherent in static grounding methods.

### 6. Conclusion

In this work, we propose Visual Semantic Confidence mechanism to construct accurate visual grounding without relying on external tools. Building upon this, we introduce Vision-Guided Attention, a novel mechanism that leverages the derived visual grounding to steer the model's visual attention toward the most informative regions, thereby effectively mitigating hallucinations in MLLMs. Moreover, it requires only a single forward pass per token, incurs negligible additional inference cost, and is compatible with FlashAttention.

### References

- [1] Shuai Bai, Keqin Chen, Xuejing Liu, Jialin Wang, Wenbin Ge, Sibo Song, Kai Dang, Peng Wang, Shijie Wang, Jun Tang, et al. Qwen2.5-vl technical report. *arXiv preprint arXiv:2502.13923*, 2025. 5
- [2] Cong Chen, Mingyu Liu, Chenchen Jing, Yizhou Zhou, Fengyun Rao, Hao Chen, Bo Zhang, and Chunhua Shen. Perturbollava: Reducing multimodal hallucinations with perturbative visual training. In *ICLR*, 2025. 2
- [3] Shiqi Chen, Tongyao Zhu, Ruochen Zhou, Jinghan Zhang, Siyang Gao, Juan Carlos Niebles, Mor Geva, Junxian He, Jiajun Wu, and Manling Li. Why is spatial reasoning hard for vlms? an attention mechanism perspective on focus areas. In *ICML*, 2025. 2, 3
- [4] Tri Dao, Dan Fu, Stefano Ermon, Atri Rudra, and Christopher Ré. Flashattention: Fast and memory-efficient exact attention with io-awareness. In *NeurIPS*, pages 16344–16359, 2022. 2
- [5] Jinghan He, Kuan Zhu, Haiyun Guo, Junfeng Fang, Zhenglin Hua, Yuheng Jia, Ming Tang, Tat-Seng Chua, and Jinqiao Wang. Cracking the code of hallucination in lvlms with vision-aware head divergence. In ACL, 2025. 2
- [6] Qidong Huang, Xiaoyi Dong, Pan Zhang, Bin Wang, Conghui He, Jiaqi Wang, Dahua Lin, Weiming Zhang, and Nenghai Yu. Opera: Alleviating hallucination in multimodal large language models via over-trust penalty and

- retrospection-allocation. In CVPR, pages 13418–13427, 2024. 2
- [7] Nicholas Jiang, Anish Kachinthaya, Suzanne Petryk, and Yossi Gandelsman. Interpreting and editing vision-language representations to mitigate hallucinations. In *ICLR*, 2025. 2
- [8] Seil Kang, Jinyeong Kim, Junhyeok Kim, and Seong Jae Hwang. See what you are told: Visual attention sink in large multimodal models. In *ICLR*, 2025. 2, 4
- [9] Sicong Leng, Hang Zhang, Guanzheng Chen, Xin Li, Shijian Lu, Chunyan Miao, and Lidong Bing. Mitigating object hallucinations in large vision-language models through visual contrastive decoding. In CVPR, pages 13872–13882, 2024.
- [10] Li Li, Jiashu Qu, Linxin Song, Yuxiao Zhou, Yuehan Qin, Tiankai Yang, and Yue Zhao. Treble counterfactual vlms: A causal approach to hallucination. In *FEMNLP*, pages 18423– 18434, 2025. 2
- [11] Yifan Li, Yifan Du, Kun Zhou, Jinpeng Wang, Wayne Xin Zhao, and Ji-Rong Wen. Evaluating object hallucination in large vision-language models. In *EMNLP*, pages 292–305, 2023. 5, 1
- [12] Zhuowei Li, Haizhou Shi, Yunhe Gao, Di Liu, Zhenting Wang, Yuxiao Chen, Ting Liu, Long Zhao, Hao Wang, and Dimitris N Metaxas. The hidden life of tokens: Reducing hallucination of large vision-language models via visual information steering. In *ICML*, 2025. 2
- [13] Tsung-Yi Lin, Michael Maire, Serge Belongie, James Hays, Pietro Perona, Deva Ramanan, Piotr Dollár, and C Lawrence Zitnick. Microsoft coco: Common objects in context. In ECCV, pages 740–755, 2014. 1
- [14] Haotian Liu, Chunyuan Li, Yuheng Li, and Yong Jae Lee. Improved baselines with visual instruction tuning. In CVPR, pages 26296–26306, 2024. 5
- [15] Haotian Liu, Chunyuan Li, Yuheng Li, Bo Li, Yuanhan Zhang, Sheng Shen, and Yong Jae Lee. Llava-next: Improved reasoning, ocr, and world knowledge, 2024. 5
- [16] Shi Liu, Kecheng Zheng, and Wei Chen. Paying more attention to image: A training-free method for alleviating hallucination in lvlms. In ECCV, pages 125–140, 2024. 1, 2,
- [17] Wenqi Liu, Xuemeng Song, Jiaxi Li, Yinwei Wei, Na Zheng, Jianhua Yin, and Liqiang Nie. Mitigating hallucination through theory-consistent symmetric multimodal preference optimization. *arXiv preprint arXiv:2506.11712*, 2025. 1, 2
- [18] Woohyeon Park, Woojin Kim, Jaeik Kim, and Jaeyoung Do. Second: Mitigating perceptual hallucination in visionlanguage models via selective and contrastive decoding. In *ICML*, 2025. 4
- [19] Peng Qi, Yuhao Zhang, Yuhui Zhang, Jason Bolton, and Christopher D Manning. Stanza: A python natural language processing toolkit for many human languages. In ACL, pages 101–108, 2020. 7, 2
- [20] Anna Rohrbach, Lisa Anne Hendricks, Kaylee Burns, Trevor Darrell, and Kate Saenko. Object hallucination in image captioning. In *EMNLP*, pages 4035–4045, 2018. 6, 1
- [21] Pritam Sarkar, Sayna Ebrahimi, Ali Etemad, Ahmad Beirami, Sercan O Arik, and Tomas Pfister. Mitigating ob-

- ject hallucination in mllms via data-augmented phrase-level alignment. In *ICLR*, 2025. 1, 2
- [22] Junyang Wang, Yuhang Wang, Guohai Xu, Jing Zhang, Yukai Gu, Haitao Jia, Jiaqi Wang, Haiyang Xu, Ming Yan, Ji Zhang, et al. Amber: An Ilm-free multi-dimensional benchmark for mllms hallucination evaluation. arXiv preprint arXiv:2311.07397, 2023. 6, 1
- [23] Kaishen Wang, Hengrui Gu, Meijun Gao, and Kaixiong Zhou. Damo: Decoding by accumulating activations momentum for mitigating hallucinations in vision-language models. In *ICLR*, 2025. 2
- [24] Wenyi Xiao, Ziwei Huang, Leilei Gan, Wanggui He, Haoyuan Li, Zhelun Yu, Fangxun Shu, Hao Jiang, and Linchao Zhu. Detecting and mitigating hallucination in large vision language models via fine-grained ai feedback. In *AAAI*, pages 25543–25551, 2025. 1, 2
- [25] Chunzhao Xie, Tongxuan Liu, Lei Jiang, Yuting Zeng, Yunheng Shen, Weizhe Huang, Jing Li, Xiaohua Xu, et al. Tarac: Mitigating hallucination in lvlms via temporal attention real-time accumulative connection. *arXiv preprint arXiv:2504.04099*, 2025. 1, 2, 5, 6
- [26] Tianyun Yang, Ziniu Li, Juan Cao, and Chang Xu. Understanding and mitigating hallucination in large vision-language models via modular attribution and intervention. In *ICLR*, 2025.
- [27] Hao Yin, Guangzong Si, and Zilei Wang. Clearsight: visual signal enhancement for object hallucination mitigation in multimodal large language models. In CVPR, pages 14625– 14634, 2025. 1, 2, 6
- [28] Hao Yin, Guangzong Si, and Zilei Wang. Lifting the veil on visual information flow in mllms: Unlocking pathways to faster inference. In *Proceedings of the Computer Vision and Pattern Recognition Conference*, pages 9382–9391, 2025.
- [29] Shukang Yin, Chaoyou Fu, Sirui Zhao, Tong Xu, Hao Wang, Dianbo Sui, Yunhang Shen, Ke Li, Xing Sun, and Enhong Chen. Woodpecker: Hallucination correction for multimodal large language models. *Science China Information Sciences*, 67(12):220105, 2024. 2
- [30] Ce Zhang, Zifu Wan, Zhehan Kan, Martin Q Ma, Simon Stepputtis, Deva Ramanan, Russ Salakhutdinov, Louis-Philippe Morency, Katia Sycara, and Yaqi Xie. Self-correcting decoding with generative feedback for mitigating hallucinations in large vision-language models. In *ICLR*, 2025. 2
- [31] Zhi Zhang, Srishti Yadav, Fengze Han, and Ekaterina Shutova. Cross-modal information flow in multimodal large language models. In *CVPR*, pages 19781–19791, 2025. 1
- [32] Jianfei Zhao, Feng Zhang, Xin Sun, and Chong Feng. Crossimage contrastive decoding: Precise, lossless suppression of language priors in large vision-language models. *arXiv* preprint arXiv:2505.10634, 2025. 2
- [33] Jianfei Zhao, Feng Zhang, Xin Sun, and Chong Feng. Aligning attention distribution to information flow for hallucination mitigation in large vision-language models, 2025.
- [34] Jianfei Zhao, Feng Zhang, Xin Sun, Lingxing Kong, Zhixing Tan, and Chong Feng. Cross-layer vision smoothing: Enhancing visual understanding via sustained focus on key

- objects in large vision-language models. arXiv preprint arXiv:2509.12897, 2025. 1, 2, 4
- [35] Linxi Zhao, Yihe Deng, Weitong Zhang, and Quanquan Gu. Mitigating object hallucination in large vision-language models via image-grounded guidance. In *ICML*, 2025. 2
- [36] Lanyun Zhu, Deyi Ji, Tianrun Chen, Peng Xu, Jieping Ye, and Jun Liu. Ibd: Alleviating hallucinations in large vision-language models via image-biased decoding. In *CVPR*, pages 1624–1633, 2025. 2
- [37] Xin Zou, Yizhou Wang, Yibo Yan, Yuanhuiyi Lyu, Kening Zheng, Sirui Huang, Junkai Chen, Peijie Jiang, Jia Liu, Chang Tang, et al. Look twice before you answer: Memoryspace visual retracing for hallucination mitigation in multimodal large language models. In *ICML*, 2025. 2, 4

# Tell Model Where to Look: Mitigating Hallucinations in MLLMs by Vision-Guided Attention

# Supplementary Material

## A. Detailed Experimental Setup

### A.1. Benchmarks

In order to validate the effectiveness of our method in mitigating hallucination, we evaluate its performance on three widely-used multimodal hallucination benchmarks: one generative benchmarks (CHAIR [20]), one discriminative benchmark (POPE [11]), and one hybrid benchmark (AMBER [22]).

**CHAIR.** CHAIR evaluates the proportion of hallucinated objects, which are generated by the model but not present in the reference annotations. Following prior works, we randomly select 500 images from the MSCOCO [13] dataset as the test set. We additionally select another 500 images to construct a validation set for hyperparameter tuning. This benchmark includes two metrics: CHAIRs and CHAIRi, defined as follows:

$$CHAIRs = \frac{|Hallucinated Objects|}{|All Objects|},$$

$$CHAIRi = \frac{|Hallucinated Captions|}{|All Captions|}$$
(16)

**POPE.** POPE is a widely adopted benchmark for evaluating object hallucinations by prompting LVLMs to identify whether a specific object is present in the image. It comprises three distinct datasets: *MSCOCO*, *A-OKVQA*, and *GQA*. Each dataset uses three different negative sampling settings: *Random*, *Popular*, and *Adversarial*. Each subset includes 3,000 questions and 500 images. Accuracy and F1 score are used as the primary evaluation metrics.

**AMBER.** AMBER combines generative and discriminative tasks, and is evaluated on a curated set of 1,004 images. In addition to image captioning, it includes 14,216 questions designed to assess hallucinations in object, attribute, and relation recognition. AMBER contians mulitple metrics: CHAIR, Cover, Hal, Cog. It provides an annotated objects list  $A_{obj} = obj_1^A, obj_2^A, \cdots, obj_n^A$ , and the generated objects are labeled as  $R'_{obj}$ . Each metric is calculated

as follows:

$$CHAIR = 1 - \frac{\operatorname{len}(R'_{obj} \cap A_{obj})}{\operatorname{len}(R'_{obj})},$$

$$Cover = \frac{\operatorname{len}(R'_{obj} \cap A_{obj})}{\operatorname{len}(A_{obj})},$$

$$Hal = \frac{\{CHAIR > 0\}}{\{All \ Caps\}},$$

$$Cog = \frac{\operatorname{len}(R'_{obj} \cap H_{obj})}{\operatorname{len}(R'_{obj})},$$

$$(17)$$

where  $H_{obj}$  denotes the set of hallucinated target objects generated by the LVLMs, and  $All\ Caps$  refers to all generated captions.

#### A.2. Baselines

We select three existing visual attention-based dehallucination methods for comparative analysis:

- PAI [16]: This method directly amplifies the model's attention weights on visual tokens and further enhances visual features using contrastive decoding. To facilitate a fair comparison of visual attention optimization, we denote the variants with and without contrastive decoding as PAI<sub>CD</sub> and PAI, respectively. We set the visual attention augmentation coefficient  $\alpha$  to 0.5 and apply visual attention augmentation starting from the layer specified by our method. PAI<sub>CD</sub> has a hyperparameter  $\gamma=1.1$  and employs adaptive plausibility constraints with  $\beta=0.1$ .
- VAF [27]: Similar to PAI, VAF directly scales up visual attention; however, it also suppresses attention on instruction tokens. We set  $\beta=0.1$ ,  $\alpha=0.15$ , and activate this method from layer 9 to layer 14 (counting from 0).
- TARAC [25]: This method quantifies the importance of visual tokens based on attention distributions from previous generation steps and utilizes this information to strengthen the model's focus on relevant visual tokens at the current step. We set  $\beta = 0.5$ ,  $\alpha = 0.5$ , and activate this method from layer 9 to layer 15 (counting from 0).

Note: The same parameters may have different meanings across methods. For specific details, please refer to the original papers.

### A.3. Implementation Details

Following the established practice of PAI, we determine the starting layer for VGA based on the *BOS* attention, which is discussed in Section B. Specifically, the starting layers are set as follows (with layers numbered from 0): layer 2

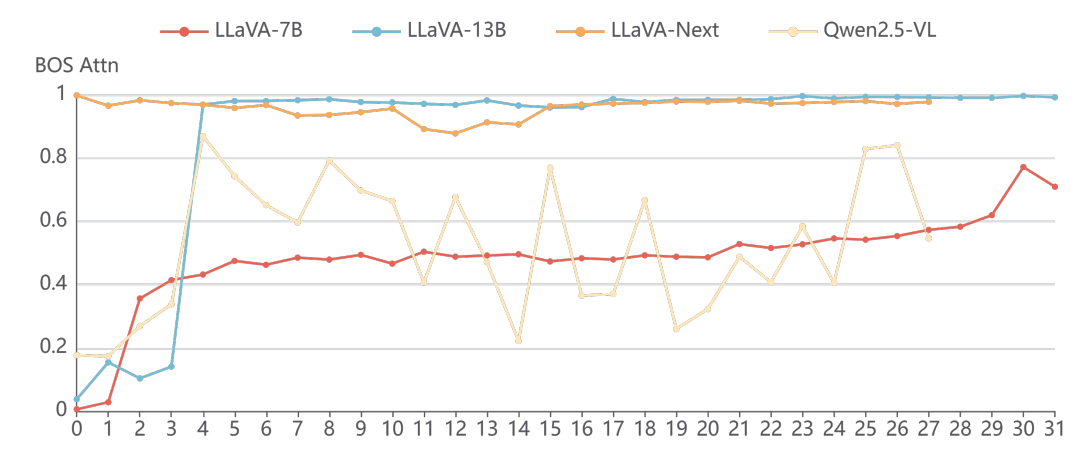


Figure 10. The model's attention to the BOS token in each layer.

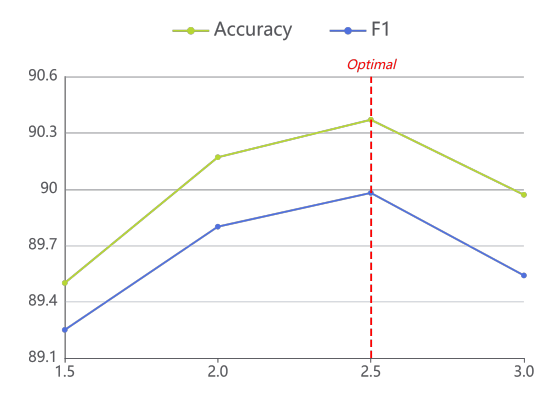


Figure 11. Effectiveness of  $\gamma$  in MSCOCO's Random set

for LLaVA-1.5, layer 0 for LLaVA-Next, and layer 4 for Qwen2.5-VL. We terminate VGA application at the middle of the model: at layer 24 for LLaVA-1.5-13B and at layer 16 for all other models. We adopt the default settings of  $\gamma=0.2$  and  $\lambda=0.02$ . For the larger model (LLaVA-1.5-13B) and visually simpler tasks (POPE), we increase  $\gamma$  to 0.25 to apply stronger vision guidance. Stanza [19] is utilized to extract objects mentioned in the question. We employ greedy decoding for next token prediction and set the maximum generation length to 512. All experiments are conducted using a single NVIDIA A800-40G GPU.

### B. The Starting Layer of VGA

In self-attention mechanisms, a "sink" phenomenon [8, 33] exists—where the model abnormally focuses its attention on a few individual tokens. PAI [16] observes that the BOS token carries very limited information yet consistently receives disproportionately high attention. Consequently, when the BOS token receives excessively high attention from the model, it serves as an appropriate trigger to enhance the model's visual attention. Following the approach

Table 5. Ablation study on CHAIR benchmark.

Setting	Cs	Ci	F1
VGA w/o Head Balancing w/o Early Termination	<b>29.8</b> 34.6 32.6		

of PAI, we analyze the BOS attention patterns across different models to determine the optimal starting layer for VGA. We apply max pooling across all attention heads. The analysis results on the image captioning task are shown in Figure 10. Based on our observations, we set the starting layer of VGA for different MLLMs as follows: layer 2 for LLaVA-1.5-7B, layer 4 for LLaVA-1.5-13B, layer 0 for LLaVA-Next, and layer 4 for Qwen2.5-VL.

## C. Ablation Study

Considering the functional diversity across attention heads, VGA employs head balancing by applying stronger guidance to heads with weaker visual features and lighter guidance to those that already exhibit strong visual functionality. Additionally, since visual understanding in MLLMs primarily occurs in the early to middle layers, we terminate visual attention guidance at an intermediate layer of the model. We conduct ablation studies on both of these design choices, and the results are presented in Table 5. Head balancing preserves the model's original visual capabilities while incorporating additional vision-guidance, thereby achieving improved performance. Meanwhile, the early exit mechanism prevents visual guidance from being applied during nonvisual understanding stages, maintaining consistency with the model's inherent behavioral characteristics. In short, both the head balancing and early termination modules contribute positively to performance.

Table 6. Effectiveness of  $\gamma$  and  $\lambda$  in CHAIR's validation set.

Setting	Cs	F1
Vanilla	49.6	76.5
$\gamma = 0.15, \lambda = 0.01$	41.6	77.5
$\gamma = 0.15, \lambda = 0.02$	43.4	76.8
$\gamma=0.15, \lambda=0.04$	43.6	77.1
$\gamma = 0.20, \lambda = 0.01$	26.2	76.4
$\gamma = 0.20, \lambda = 0.02$	32.8	77.7
$\gamma = 0.20, \lambda = 0.04$	38.6	77.9
$\gamma = 0.25, \lambda = 0.01$	10.0	68.7
$\gamma=0.25, \lambda=0.02$	11.8	69.1
$\gamma=0.25, \lambda=0.04$	19.8	71.8

### D. The evaluation of TTFT

We evaluate the inference overhead of VGA using LLaVA-1.5-7B on the AMBER benchmark, with Time to First Token (TTFT) as the primary metric. We randomly select 1,000 samples and report the average TTFT over three runs. VGA achieves an average TTFT of 0.1149 second/sample, compared to 0.1101 second/sample for the vanilla baseline. This corresponds to only a 4.36% increase in inference latency relative to the vanilla approach.

# E. Hyperparameters

 $\gamma$  controls the strength of visual guidance, while  $\lambda$  controls the penalty strength on already-generated content in image captioning tasks. We perform a grid search for  $\gamma$  on the POPE benchmark, as shown in Figure 11. Additionally, we conduct a grid search over both  $\gamma$  and  $\lambda$  on the CHAIR benchmark, with results presented in Table 6. We observe that for tasks like POPE, which require focusing on a single visual region, stronger visual guidance is beneficial. In contrast, for image captioning tasks that demand broader attention across multiple visual regions, overly strong guidance can restrict the model's capacity. Therefore, we set  $\gamma=0.25$  on the POPE benchmark and  $\gamma=0.2$  on other benchmarks. Furthermore, for image captioning, we select  $\lambda=0.02$  based on a balanced consideration of hallucination rate and F1 score.